Accepted Manuscript

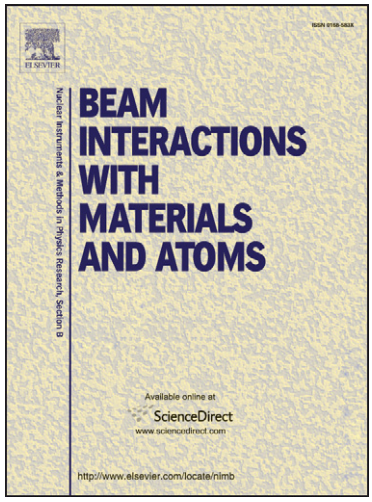

A Detailed Study of the d+^{10}B System for Nuclear Reaction Analysis. Part A: The ^{10}B(d,p)^{11}B Reaction in the Energy Region $E_{d,\,lab}$= 900-2000 keV

M. Kokkoris, V. Foteinou, G. Provatas, A. Kontos, N. Patronis, C.T. Papadopoulos, R. Vlastou, P. Misaelides, A. Lagoyannis, S. Harissopulos

PII: S0168-583X(07)01325-0
DOI: 10.1016/j.nimb.2007.07.003
Reference: NIMB 54942

To appear in: *Nucl. Instr. and Meth. in Phys. Res. B*

Received Date: 4 April 2007
Revised Date: 7 June 2007
Accepted Date: 3 July 2007

Please cite this article as: M. Kokkoris, V. Foteinou, G. Provatas, A. Kontos, N. Patronis, C.T. Papadopoulos, R. Vlastou, P. Misaelides, A. Lagoyannis, S. Harissopulos, A Detailed Study of the d+^{10}B System for Nuclear Reaction Analysis. Part A: The ^{10}B(d,p)^{11}B Reaction in the Energy Region $E_{d,\,lab}$= 900-2000 keV, *Nucl. Instr. and Meth. in Phys. Res. B* (2007), doi: 10.1016/j.nimb.2007.07.003

A Detailed Study of the d+^{10}B System for Nuclear Reaction Analysis. Part A: The ^{10}B(d,p)^{11}B Reaction in the Energy Region $E_{d,\,lab}$ = 900-2000 keV

M. Kokkoris[1,a], V. Foteinou[a], G. Provatas[a], A. Kontos[a], N. Patronis[a], C.T. Papadopoulos[a], R. Vlastou[a], P. Misaelides[b], A. Lagoyannis[c], S. Harissopulos[c]

[a] *Department of Physics, National Technical University of Athens, Zografou Campus 157 80, Athens, Greece*

[b] *Department of Chemistry, Aristotle University of Thessaloniki, GR-54124 Thessaloniki, Greece*

[c] *Institute of Nuclear Physics, TANDEM Accelerator, N.C.S.R. 'Demokritos', Aghia Paraskevi 153 10, Athens, Greece*

Abstract

The differential cross sections of the ^{10}B(d,$p_{0,1,2,3,4\text{-}5,6}$) reactions for the determination of the depth distribution of boron in near-surface layers of materials have been determined in the projectile energy region $E_{d,\,lab}$ = 900-2000 keV. The experiment was carried out in energy steps of 25 keV and for eight detector angles between 135° and 170° (in steps of 5°). The obtained experimental data are suitable for Nuclear Reaction Analysis (NRA) studies. A qualitative discussion of the observed cross section variations through the strong influence of overlapping resonances in the d+^{10}B system is also presented.

Keywords: Nuclear Reaction Analysis; Boron; Reaction cross section; Backscattering

---

[1] Corresponding author, e-mail: kokkoris@central.ntua.gr

PACS No: 25.45.-z, 82.80.Yc, 25.45.De

1. Introduction

The quantitative determination of boron is very important in many technical applications, including dopant depth profiling in semiconductors, quality control of boron nitride thin films, as well as, in the plasma technology and environmental research. The determination of the boron distribution, especially on heavy substrates and/or in the presence of other light elements, presents a strong analytical challenge for all ion beam analysis (IBA) techniques.

Nuclear Reaction Analysis (NRA) is well established as one of the principal IBA methods nowadays, due to its high isotopic selectivity, enhanced sensitivity for many elements, capability of least destructive depth profiling, and the possibility of simultaneous analysis of more than one light element in near-surface layers of materials [e.g. 1]. As NRA can also be used to quantify individual light isotopes absolutely, and can provide depth profiles for them with nanometer resolution, it is probably the most suitable ion beam analysis technique for the determination of the concentration and the depth profile of light elements in complex matrices. However, in certain cases, the implementation of NRA in light element depth profiling is impeded by the lack of adequate or reliable differential cross section data over a wide range of energies and steep backward detector angles in literature (as in the cases of ^{10,11}B).

Natural boron is comprised of 81.1% ^{11}B and 19.9% ^{10}B. Thus, as far as NRA is concerned, the analytical study of both isotopes is imperative. In the case of ^{10}B, only a few pioneer works have been presented in the field of charged particle spectroscopy in the past, investigating the (^{3}He,p) [2, 3], (p,α) [4, 5], and (α,p) [6, 7] reactions. The last one seems to be best suited for ^{10}B profiling, mainly due to its relatively high cross section [6]. Nevertheless,

to the authors' best knowledge, with the exception of one old report on the (d,α) reaction [8], there is no other contribution available in literature for the d+^{10}B system at low energies (in the backscattering geometry) suitable for NRA purposes. This surprising lack of data, especially concerning the ^{10}B(d,p) reaction, can be partly attributed to the requirement for thick, high-resolution silicon surface barrier detectors (not available in the past), due to the relatively high energy protons emitted from this reaction. On the other hand, the use of a deuterium probing beam (rather than protons or helium), offers critical advantages for NRA studies, due to: a) the simultaneous excitation of most light elements (e.g. O, N, C, F, Al, Mg and S) usually co-existing in complex matrices, and b) the enhanced sensitivity and accuracy, mainly due to the generally large cross sections of the deuteron-induced nuclear reactions. These advantages are, of course, offered at the expense of background interference in certain cases (e.g. peak overlaps, 3-body reaction kinematics). Also, certain radiation safety precautions are mandatory due to the emitted neutrons from (d,n) reactions (on the target elements and structural materials), and/or deuteron breakup (for deuteron beam energies above 2.2 MeV).

Thus, the present work aims at contributing to the field of deuteron induced reactions., through the study of the differential cross sections of ^{10}B(d,$p_{0,1,2,3,4\text{-}5,6}$), in the projectile energy region $E_{d,\,lab}$ = 900-2000 keV (in steps of 25 keV) and for detector angles 135° to 170° (in steps of 5°), suitable for NRA purposes. The results from the present work could be directly incorporated in widely used NRA algorithms (e.g. SIMNRA [9], WINDF [10])

2. Experimental Setup and Procedure

The experiments were performed using the deuteron beam of the 5.5 MV TN11 Tandem Accelerator of N.C.S.R. "Demokritos", Athens, Greece. The deuterons, accelerated

to $E_{d,lab}$=900-2000 keV in steps of 25 keV, were led to a scattering chamber of large dimensions.

The final ion energy of the deuteron beam was determined by nuclear magnetic resonance measurements (NMR) with an estimated ripple of 1.6±0.4 keV, as verified by the 991.9 keV resonance of the ^{27}Al(p,γ) reaction at the beginning and at the end of the experiment, using a 56% (relative efficiency) HPGe detector. The maximum error in the determination of $E_{d,lab}$ was thus estimated to be at most 2 keV (in order to include any possible deviations of the magnet at higher energies). The maximum offset determined was 3.25 keV and was thus included in the subsequent analysis. For the determination of the offset, the threshold reaction ^{16}O(d,n) was also implemented, with the use of an additional BF_3 neutron counter set at 30^o with respect to the beam axis.

The detection system consisted of four Si surface barrier detectors (Thickness: 1000 to 2000 μm; all rotating, set at 10° intervals) along with the corresponding electronics. The spectra from all the four detectors were simultaneously recorded and the procedure was repeated by turning all the Si detectors by 5° for every $E_{d,\,lab}$. The beam spot size was 2.5×2.5 mm^2, while the current on target did not exceed 100 nA during any measurement. Two liquid nitrogen traps were set on both ends of the goniometer in order to reduce the carbon build-up on the targets, while the vacuum was kept constant, as low as ~5×10^{-7} Torr.

A highly pure (>98%), isotopically enriched (94.6%) ^{10}B target deposited on a mirror polished thick tantalum backing was used for the experiments. The thickness of the target (10.2 μg/cm^2 at 10% accuracy, corresponding to an energy loss of ~4-6 keV of the impinging deuterons over the whole energy range studied, taking into account oxidization and carbon contamination), as well as its high lateral homogeneity (differences less than 1.7%) were determined in the past by interferometry at the Institute for Reference Materials and Measurements (IRMM), Geel, Belgium, where the target was manufactured. The target

thickness and its corresponding uncertainty were also verified in the present work using AFM measurements, as well as ^{12}C-RBS spectra (at 8, 9 and 10 MeV) from both sides of the target (B on Ta and pure Ta respectively, via the energy difference of the Ta surface edge), along with data from literature for the determination of the oxygen (via the $^{16}O(d,p_0)$ reaction [11]) and of the carbon content (via the $^{12}C(d,p_0)$ reaction [12]) from the obtained NRA spectra. Despite the many sources of uncertainty in this latter method (stopping power of impinging carbon ions, uncertainties in the NRA differential cross sections for $^{12}C(d,p_0)$ and $^{16}O(d,p_0)$ etc), the obtained results corroborated with the manufacturer's analysis within error. After every ~10 steps in beam energy, the beam spot position was slightly changed on the target (circular, with a diameter of ~10 mm) in order to avoid excessive carbon buildup and/or target deterioration.

The target was placed at a distance of ~8.5 cm from the detectors. An absorber foil of 50 μm kapton was used to impede elastically scattered deuterons from reaching the detectors. Additionally, orthogonal slits (~4.5 x 10 mm^2) were placed in front of the detectors in order to reduce the angular uncertainty (~±1.5^o), while allowing an adequate effective solid angle to be subtended by the detectors. This effective solid angle (along with the energy resolution of the detectors) was determined via a 81.1 nCi triple α-source (^{241}Am/^{239}Pu/^{244}Cm, IAEA certified, at 4% accuracy), placed at the exact location of the beam spot (and being of approximately the same size), and was found to vary between ~6x10^{-3} and ~8x10^{-3} sr (for different detectors). These values were also verified by deuteron-induced Rutherford backscattering measurements (d-RBS) using high purity mechanically polished thick aluminum and gold foils as targets (d-RBS spectra taken at E_d=1, 1.5 and 2 MeV). Using SIMNRA (v. 5.02) for the analysis of the thick-target d-RBS spectra [9], both Andersen-Ziegler [13] and Ziegler-Biersack-Littmark (ZBL, [14]) stopping power data for deuterons were implemented, as incorporated in the algorithm. The obtained simulated results for a minimization window set relatively close to

the surface (in order to exclude energy straggling effects) differed by only 0.6-1.6% for both targets (over the whole energy region studied). Given this agreement, ZBL stopping power data were adopted for the calculations. The total estimated error for the product Q*Ω varied between ~4-7% (pending on the detector). The statistical error also varied between ~1-5%, with the (d,p_3) being the least favorable case in the energy interval studied (mainly due to the high-induced background at low energies).

Two different algorithms were implemented for peak fitting/integration and background subtraction, yielding results within 1-2%. For the charge measurements (charge collection and subsequent current integration) the whole chamber was electrically isolated from the beam line and voltage suppression of ~300 V was applied on both the collimator set and on target. A typical experimental spectrum taken at 160° and $E_{d,lab}$=1419 keV is presented in Fig. 1, along with the corresponding peak identification. The broad background appearing under the p_2 and p_3 peaks is related to the ^{10}B(d,α) reaction (3-body kinematics), which is separately analyzed in part B. This structure is in details demonstrated in the smaller image embedded in Fig. 1.

3. Analysis and Discussion

The determination of the differential cross section values was carried out following the formula for absolute measurements:

$$\left(\frac{d\sigma}{d\Omega}\right)_{\theta} = \frac{Y}{Q * \Omega * Nt_i}$$

where Y corresponds to the experimental yield (integrated peak counts), Q to the number of impinging deuteron ions, Ω to the solid angle subtended by the detector set at angle θ, and Nt_i to the ^{10}B target thickness in at/cm^2. The combined errors, varying between ~11-16% (for different levels), included uncertainties in the product Q*Ω, in the target thickness, in peak integration, as well as, statistical uncertainties, and corresponded to ±1σ accuracy. The total

experimental uncertainty was calculated following standard error propagation formulas. The main source of error was undoubtedly, thus, related to the determination of the ^{10}B content in the isotopically enriched target. Concerning the thickness of the target, repeated AFM measurement revealed that this was of the same order of magnitude with the roughness of the polished tantalum substrate. Thus, the target thickness uncertainty could not be reduced below 10% of the nominal value.

The data obtained in the present study are presented, along with the experimental errors, in fig. 2a-g (for the backward angles 135º, 140º, 145º, 150º, 160º, 165º and 170º respectively). In each figure all the resolved peaks are presented (p_0, p_1, p_2, p_3, p_{45}, p_6). The use of the thick kapton foil in front of the detectors impeded the kinematic separation of p_4 from p_5 (corresponding to the excited states at 6742.9 keV and 6791.8 keV in ^{11}B respectively). In this case only combined differential cross sections are reported, which are essentially significantly larger than the ones reported for all the other levels. With the exception of p_{45}, all the differential cross sections obtained were generally lower than ~2 mb/sr. It is evident from fig. 2a-g that the angular variation of the differential cross section values for all the levels is rather slow, over the whole energy range studied. This greatly facilitates NRA measurements, allowing – to a good approximation – a linear interpolation of the cross section values for intermediate detector angles. This is a common problem encountered in goniometers with fixed detector settings, when one implements NRA cross section data from literature, taken at slightly different detector angles. Thus boron profiling can be performed with high accuracy in such setups, following a proper interpolation of the data reported in the present work.

In an attempt to study the effect of the resonance mechanism in the differential cross sections of all the levels in more detail, the obtained results for the characteristic detector angle at 155.0º±1.4º are presented in fig. 3a-f. The energy range studied in the present work

corresponds to an excitation energy between 25936 keV and 26853 keV (c.m. system) of the compound nucleus $^{12}C^{*}$. In this range, the effects of the broad resonances at 25950 keV (Γ=0.4 MeV) [15, 16] and at 26800 keV (Γ=270 keV) are evident. Moreover, a possible strong influence of the much broader states at 25400 keV (Γ=2 MeV) and at 27000±300 keV (Γ=1.4 MeV), which are out of the covered energy range, cannot be excluded. These overlapping resonances cause a strong increase of the measured p_2, p_3, p_6 cross section values in the energy range $E_{d,\,lab}$ ~900-1400 keV. The trend is reversed in the case of p_0, while the p_1 cross section values remain relatively unaffected. In the region $E_{d,\,lab}$ ~1600-2000 keV, however, p_0, and p_2 cross section values exhibit an increase, while the corresponding ones for p_1, p_3, and p_6 demonstrate an opposite behavior. All these resonant effects are rather smeared out in the case of the combined p_{45} values, as should be expected. Thus, it is interesting to note at this point that a possible evaluation of deuteron induced reactions in ^{10}B (based both on the available experimental points and on theoretical models) presents strong theoretical challenges. Among many reasons that enhance the complexity of the problem (such as the co-existence of many open reaction channels, the electric charge asymmetry of the deuteron, the effects of a multiple projectile-target exchange of nucleons, the existence of direct exchange processes such as knock-out and stripping), the problem of taking into account overlapping resonances [17] seems to be of vital importance. At such high excitation energies of the compound nucleus, even the assigned J^{π} values of the levels involved are doubtful [15]. It is the authors' firm belief that coordinated efforts on both fields (experimental and theoretical) are required before such a goal is accomplished.

As far as NRA measurements are concerned, it should also be noted that no real 'plateau' has been observed in the differential cross section values of any of the exit channels, over the whole energy range studied ($E_{d,\,lab}$=900-2000 keV), as shown in figs. 2 and 3. This sets certain limits to the analyzing power of the $^{10}B(d,p)$ reaction, especially for boron depth

profiling of relatively thin targets, when the accelerator beam energy is not known with high accuracy. A possible solution to this problem could be the simultaneous implementation of all the levels studied in the present work for higher statistical accuracy, along with spectra acquisition at several beam energies, or – for a given accelerator energy – the careful choice of at least two differential cross section datasets exhibiting opposite behaviors with respect to the beam energy (increasing/decreasing). Alternatively, one can use the rather stable values of p_1 in the energy range $E_{d,\,lab}$~900-1200 keV for most steep backward angles between 135º and 170º.

All the obtained differential cross section values for p_0 – p_6 are presented – following the usual convention – in tables 1-6 respectively, along with the corresponding combined errors. The reported energy values, after the proper correction according to the results of the machine calibration presented in the previous section, correspond to the half of the target's thickness, following SRIM 2003 calculations. The results, in both graphical and tabular forms are already available to the scientific community through IBANDL (www-nds.iaea.org/ibandl/).

4. Conclusions

In the present work, a detailed study of the differential cross sections of the ^{10}B(d,p) reaction for backward angles (between 135º and 170º), and for the deuteron energy beam range $E_{d,\,lab}$~900-2000 keV, suitable for NRA purposes has been presented for the first time. Cross sections for the exit channels p_0, p_1, p_2, p_3 and p_6 have been studied independently, while combined values have also been obtained for p_4 and p_5. More than ~2000 differential cross section values have been determined for 8 different detector angles (at 5º intervals), in beam energy steps of ~25 keV. The behavior of these values with respect to the beam energy

has been explained qualitatively, via the strong influence of overlapping resonances at high excitation energies.

As a result, the ^{10}B(d,p) reaction seems to be well suited for NRA studies and IBA applications in general, especially when complex matrices containing several light elements are involved. Although the obtained cross section values are somewhat lower than the ones presented in the past for the ^{10}B(p,α) [4, 5] or the ^{10}B(α,p) [6, 7] reactions, the advantages of simultaneously exciting the most common light elements, as well as the low deuteron beam energies required, render this reaction an important candidate for boron profiling studies.

References

[1] J. R. Tesmer and M. Nastasi (eds), "*Handbook of modern ion beam materials analysis",* chapter 6, 'Nuclear Reaction Analysis: Particle – Particle Reactions' by G. Vizkelethy, chapter 7, 'Nuclear Reaction Analysis: Particle – Gamma Reactions' by J. –P. Hirvonen, Materials Research Society, Pittsburgh, PA, (1995).

[2] J.P. Schiffer, T.W. Bonner, R.H. Davis and W.Prosser, *Phys. Rev*. **104** (1956) 10

[3] L.C. McIntyre Jr., J.A. Leavitt, M.D. Ashbaugh, J. Borgardt, E. Andrade, J. Rickards, A. Oliver, *Nucl. Instr. Meth.* **B118** (1996) 219.

[4] H.J. Kim, W.T. Milner and F.K. McGowan, *Nuclear Data Tables* **A3** (1967) 123.

[5] J.G.Jenkin, L.G.Earwaker and E.W.Tinterton, *Nucl. Phys.*, **50** (1964), 517.

[6] G. Giorginis, A. Crametz, P. Misalides, and M. Conti, *Nucl. Instr. Meth.* **B118** (1996) 224.

[7] H. Chen et al., *Nucl. Instr. Meth*. **B211** (2003) 1.

[8] K.H. Purser and B.H. Wildenthal, *Nucl. Phys.*, **44** (1963), 22.

[9] M. Mayer, *"SIMNRA, a Simulation Program for the Analysis of NRA, RBS and ERDA"*, Proceedings of the 15th CAARI, J. L. Duggan and I. L. Morgan (eds), AIP

Conf. Proc. **475**, (1999) 541.

[10] C Jeynes, N P Barradas, P K Marriott, G Boudreault, M Jenkin, E Wendler and R P Webb, *J. of Phys.* **D36, 7** (2003) R97-R126.

[11] A. Gurbich, S. Molodtsov, *Nucl. Instr. Meth.* **B226** (2004) 637.

[12] E. Kashy, R.R. Perry and J.R. Risser, *Phys. Rev*. **117** (1960), 1289.

[13] H.H. Andersen and J.F. Ziegler, *"Hydrogen Stopping Powers and Ranges in All Elements"*, vol. 3 of *"The Stopping and Ranges of Ions in Matter"*, Pergamon Press, NewYork, 1977.

[14] J.F. Ziegler, J.P. Biersack and U. Littmark, *"The Stopping and Range of Ions in Solids"*, Pergamon Press, New York (1985).

[15] Richard B. Firestone, Virginia S. Shirley, Coral M. Baglin, S.Y. Frank Chu, and Jean Zipkin, 'Table of Isotopes', 8th Edition, Vol. 1, John Wiley & Sons, Inc., New Jersey (1996).

[16] F. Ajzenberg-Selove, *Nucl. Phys.*, **A506** (1990) 1, *Nucl. Phys.*, **A336** (1980) 1, and *Nucl. Phys.*, **A490** (1988) 1.

[17] A.F. Gurbich, IAEA Report of the Advisory Group Meeting on Long Term Needs for Nuclear Data Development (Vienna, 28/11-1/12, 2000).

Table Captions

Tables 1-6. Tabulated differential cross sections (mb/sr) of the $^{10}B(d,p_0)^{11}B$, $^{10}B(d,p_1)^{11}B$, $^{10}B(d,p_2)^{11}B$, $^{10}B(d,p_3)^{11}B$, $^{10}B(d,p_{45})^{11}B$, and $^{10}B(d,p_6)^{11}B$ reactions, measured in the $E_{d,\,lab}$ region 900-2000 keV, at detection angles between 135° and 170° (values are omitted when the cross section could not be determined accurately). The corresponding combined cross section errors at ±1σ accuracy are also included.

Figure Captions

Figure 1. Experimental spectrum taken at 160° and $E_{d,\ lab}$=1419 keV, along with the corresponding peak identification.

Figure 2a-g. Differential cross section values (mb/sr) of the $^{10}B(d,p_{0,1,2,3,45,6})^{11}B$ reactions at 135°, 140°, 145°, 150°, 160°, 165° and 170° respectively, for $E_{d,\ lab}$=900-2000 keV. The combined experimental errors are included in the graphs. The errors along the x-axis (energy ripple of ±2 keV) are not visible due to the adopted scale.

Figure 3a-f. A detailed representation of differential cross section values (mb/sr) of the $^{10}B(d,p_{0,1,2,3,45,6})^{11}B$ reactions at 155°, in order to demonstrate the effect of broad resonances in the d+^{10}B system.

E_{lab} (keV)	$\sigma_{E_{lab}}$ (keV)	$(\sigma \pm d\sigma)$ (mb/sr), p_0															
		135°		140°		145°		150°		155°		160°		165°		170°	
894	2	0.59	0.07	0.56	0.07	0.57	0.07	0.54	0.07	0.50	0.05	0.47	0.05	0.45	0.05	0.46	0.05
919	2	0.65	0.08	0.60	0.07	0.58	0.07	0.56	0.07	0.50	0.05	0.47	0.05	0.51	0.05	0.47	0.05
944	2	0.62	0.08	0.61	0.07	0.59	0.07	0.57	0.07	0.53	0.06	0.48	0.05	0.49	0.05	0.47	0.05
967	2	0.64	0.08	0.63	0.08	0.60	0.07	0.54	0.07	0.50	0.05	0.48	0.05	0.49	0.05	0.44	0.05
994	2	0.66	0.08	0.63	0.08	0.60	0.07	0.55	0.07	0.51	0.06	0.47	0.05	0.49	0.05	0.45	0.05
1019	2	0.70	0.08	0.64	0.08	0.59	0.07	0.53	0.07	0.48	0.05	0.44	0.05	0.46	0.05	0.44	0.05
1044	2	0.68	0.08	0.64	0.08	0.60	0.07	0.53	0.07	0.47	0.05	0.45	0.05	0.45	0.05	0.41	0.05
1069	2	0.67	0.08	0.62	0.08	0.60	0.07	0.57	0.07	0.45	0.05	0.41	0.05	0.41	0.04	0.42	0.05
1094	2	0.67	0.08	0.76	0.09	0.59	0.07	0.54	0.07	0.45	0.05	0.51	0.05	0.40	0.04	0.40	0.04
1119	2	0.65	0.08	0.71	0.08	0.56	0.07	0.51	0.06	0.43	0.05	0.51	0.05	0.40	0.04	0.33	0.04
1144	2	0.63	0.08	0.59	0.07	0.56	0.07	0.50	0.06	0.44	0.05	0.38	0.04	0.38	0.04	0.34	0.04
1169	2	0.65	0.08	0.61	0.07	0.57	0.07	0.53	0.06	0.40	0.04	0.39	0.04	0.37	0.04	0.37	0.04
1194	2	0.66	0.08	0.63	0.08	0.58	0.07	0.52	0.06	0.44	0.05	0.39	0.04	0.38	0.04	0.35	0.04
1219	2	0.66	0.08	0.59	0.07	0.55	0.07	0.49	0.06	0.44	0.05	0.34	0.04	0.38	0.04	0.33	0.04
1244	2	0.68	0.08	0.60	0.07	0.57	0.07	0.52	0.06	0.43	0.05	0.37	0.04	0.38	0.04	0.37	0.04
1269	2	0.70	0.08	0.59	0.07	0.53	0.06	0.51	0.06	0.42	0.05	0.36	0.04	0.36	0.04	0.30	0.03

1294	2	0.68	0.08	0.59	0.07	0.54	0.07	0.49	0.06	0.40	0.04	0.36	0.04	0.37	0.04	0.33	0.04
1319	2	0.69	0.08	0.62	0.07	0.59	0.07	0.52	0.06	0.43	0.05	0.37	0.04	0.37	0.04	0.36	0.04
1344	2	0.70	0.08	0.64	0.08	0.58	0.07	0.52	0.06	0.47	0.05	0.42	0.05	0.40	0.04	0.35	0.04
1369	2	0.71	0.09	0.63	0.08	0.63	0.08	0.55	0.07	0.49	0.05	0.41	0.05	0.41	0.04	0.37	0.04
1394	2	0.74	0.09	0.70	0.09	0.65	0.08	0.58	0.07	0.50	0.06	0.44	0.05	0.42	0.05	0.38	0.04
1419	2	0.80	0.10	0.71	0.09	0.65	0.08	0.59	0.07	0.52	0.06	0.48	0.05	0.46	0.05	0.42	0.05
1444	2	0.78	0.09	0.73	0.09	0.67	0.08	0.62	0.07	0.55	0.06	0.48	0.05	0.46	0.05	0.43	0.05
1469	2	0.89	0.11	0.74	0.09	0.76	0.09	0.66	0.08	0.61	0.07	0.49	0.05	0.50	0.05	0.47	0.05
1494	2	0.89	0.11	0.81	0.10	0.72	0.09	0.70	0.09	0.62	0.07	0.56	0.06	0.55	0.06	0.52	0.06
1520	2	0.86	0.11	0.83	0.10	0.79	0.10	0.69	0.09	0.62	0.07	0.57	0.06	0.61	0.07	0.54	0.06
1545	2	0.92	0.11	0.86	0.11	0.77	0.10	0.76	0.09	0.70	0.08	0.62	0.07	0.63	0.07	0.56	0.06
1570	2	0.92	0.11	0.87	0.11	0.81	0.10	0.75	0.09	0.69	0.07	0.63	0.07	0.64	0.07	0.61	0.07
1595	2	0.96	0.12	0.88	0.11	0.84	0.10	0.80	0.10	0.74	0.08	0.68	0.07	0.66	0.07	0.64	0.07
1620	2	0.93	0.11	0.89	0.11	0.80	0.10	0.79	0.10	0.71	0.08	0.66	0.07	0.68	0.07	0.64	0.07
1645	2	0.94	0.11	0.93	0.11	0.85	0.10	0.79	0.10	0.73	0.09	0.72	0.08	0.73	0.08	0.65	0.07
1670	2	0.93	0.11	0.90	0.11	0.82	0.10	0.77	0.10	0.73	0.08	0.69	0.08	0.69	0.07	0.70	0.08
1695	2	0.96	0.12	0.91	0.11	0.87	0.11	0.86	0.10	0.74	0.08	0.72	0.09	0.76	0.08	0.72	0.08
1720	2	1.00	0.12	0.94	0.12	0.92	0.11	0.84	0.10	0.80	0.09	0.75	0.08	0.75	0.08	0.75	0.08
1745	2	1.07	0.13	1.00	0.12	0.89	0.11	0.90	0.11	0.83	0.09	0.78	0.09	0.81	0.09	0.79	0.09

1770	2	1.09	0.13	1.01	0.12	0.97	0.12	0.91	0.11	0.92	0.10	0.80	0.09	0.91	0.10	0.77	0.08
1795	2	1.01	0.12	1.07	0.13	1.02	0.13	0.90	0.11	0.96	0.10	0.84	0.09	0.91	0.10	0.87	0.09
1820	2	1.12	0.14	1.02	0.13	0.96	0.12	0.93	0.11	0.96	0.11	0.92	0.10	0.88	0.10	0.93	0.10
1845	2	1.11	0.14	1.07	0.13	1.01	0.12	1.00	0.12	0.97	0.11	0.96	0.11	0.96	0.11	0.97	0.11
1870	2	1.12	0.14	1.08	0.13	1.10	0.13	1.02	0.13	1.02	0.11	0.94	0.10	1.07	0.12	1.01	0.11
1895	2	1.17	0.14	1.19	0.14	1.11	0.14	1.07	0.13	1.04	0.11	1.05	0.11	1.12	0.12	1.08	0.12
1920	2	1.19	0.15	1.12	0.14	1.11	0.14	1.09	0.13	1.10	0.12	1.02	0.11	1.11	0.12	1.11	0.10
1945	2	1.19	0.14	1.21	0.15	1.10	0.13	1.14	0.14	1.10	0.12	1.12	0.12	1.08	0.11	1.09	0.12
1970	2	1.25	0.15	1.20	0.15	1.13	0.14	1.14	0.14	1.12	0.12	1.15	0.12	1.17	0.13	1.10	0.12
1995	2	1.28	0.16	1.16	0.14	1.12	0.14	1.12	0.14	1.11	0.12	1.08	0.12	1.11	0.12	1.13	0.12

Table 1

E_{lab} (keV)	$\sigma_{E_{lab}}$ (keV)	$(\sigma \pm d\sigma)$ (mb/sr), p_1															
		135°		140°		145°		150°		155°		160°		165°		170°	
894	2	0.207	0.027	0.207	0.027	0.197	0.026	0.191	0.025	0.179	0.021	0.170	0.020	0.186	0.021	0.186	0.021
919	2	0.202	0.026	0.177	0.023	0.199	0.026	0.203	0.026	0.199	0.023	0.176	0.020	0.192	0.022	0.158	0.019
944	2	0.25	0.03	0.225	0.029	0.207	0.026	0.203	0.026	0.182	0.021	0.186	0.022	0.180	0.021	0.187	0.022
967	2	0.23	0.03	0.215	0.029	0.209	0.027	0.178	0.023	0.180	0.021	0.178	0.021	0.190	0.022	0.180	0.021
994	2	0.199	0.027	0.23	0.03	0.214	0.027	0.205	0.026	0.183	0.021	0.193	0.022	0.203	0.023	0.188	0.022
1019	2	0.221	0.029	0.200	0.027	0.213	0.027	0.204	0.026	0.187	0.022	0.176	0.020	0.196	0.022	0.192	0.022
1044	2	0.221	0.029	0.24	0.03	0.229	0.029	0.194	0.025	0.195	0.022	0.168	0.020	0.188	0.022	0.178	0.021
1069	2	0.25	0.03	0.195	0.025	0.194	0.025	0.211	0.029	0.187	0.022	0.164	0.019	0.201	0.023	0.178	0.021
1094	2	0.194	0.026	0.208	0.027	0.191	0.024	0.202	0.025	0.187	0.022	0.212	0.024	0.180	0.021	0.195	0.022
1119	2	0.232	0.029	0.230	0.029	0.210	0.026	0.211	0.026	0.185	0.021	0.180	0.020	0.186	0.021	0.193	0.021
1144	2	0.212	0.027	0.207	0.027	0.173	0.022	0.195	0.024	0.172	0.019	0.167	0.019	0.195	0.022	0.188	0.021
1169	2	0.25	0.03	0.216	0.028	0.195	0.023	0.189	0.024	0.177	0.019	0.192	0.021	0.180	0.020	0.181	0.020
1194	2	0.26	0.03	0.220	0.028	0.213	0.026	0.201	0.025	0.192	0.021	0.172	0.019	0.176	0.020	0.190	0.021
1219	2	0.208	0.027	0.230	0.029	0.215	0.027	0.207	0.026	0.213	0.024	0.187	0.021	0.190	0.021	0.196	0.022
1244	2	0.231	0.029	0.203	0.025	0.220	0.028	0.199	0.025	0.214	0.024	0.205	0.023	0.186	0.021	0.203	0.028

1269	2	0.192	0.025	0.222	0.029	0.220	0.028	0.206	0.026	0.195	0.022	0.205	0.023	0.200	0.022	0.195	0.022
1294	2	0.212	0.027	0.210	0.027	0.226	0.029	0.220	0.027	0.187	0.022	0.221	0.025	0.203	0.022	0.220	0.024
1319	2	0.27	0.03	0.27	0.03	0.24	0.03	0.221	0.027	0.233	0.026	0.209	0.023	0.231	0.026	0.218	0.024
1344	2	0.23	0.03	0.24	0.03	0.25	0.03	0.23	0.03	0.226	0.025	0.221	0.025	0.235	0.026	0.237	0.026
1369	2	0.23	0.03	0.25	0.03	0.25	0.03	0.26	0.03	0.242	0.027	0.232	0.026	0.235	0.026	0.235	0.026
1394	2	0.27	0.03	0.27	0.03	0.25	0.03	0.26	0.03	0.27	0.03	0.236	0.026	0.252	0.028	0.26	0.03
1419	2	0.26	0.03	0.26	0.03	0.27	0.03	0.28	0.04	0.26	0.03	0.242	0.027	0.28	0.03	0.28	0.03
1444	2	0.29	0.04	0.27	0.03	0.29	0.04	0.29	0.04	0.28	0.03	0.28	0.03	0.31	0.03	0.29	0.03
1469	2	0.29	0.04	0.27	0.03	0.28	0.04	0.28	0.04	0.30	0.03	0.27	0.03	0.31	0.03	0.30	0.03
1494	2	0.31	0.04	0.29	0.04	0.31	0.04	0.29	0.04	0.29	0.03	0.28	0.03	0.30	0.03	0.34	0.04
1520	2	0.31	0.04	0.30	0.04	0.33	0.04	0.27	0.03	0.34	0.04	0.30	0.03	0.35	0.04	0.33	0.04
1545	2	0.30	0.04	0.32	0.04	0.32	0.04	0.31	0.04	0.34	0.04	0.30	0.03	0.35	0.04	0.35	0.04
1570	2	0.33	0.05	0.31	0.04	0.32	0.04	0.33	0.04	0.33	0.04	0.31	0.04	0.33	0.04	0.33	0.04
1595	2	0.28	0.04	0.33	0.04	0.28	0.04	0.31	0.04	0.31	0.03	0.31	0.03	0.34	0.04	0.35	0.04
1620	2	0.30	0.04	0.29	0.04	0.29	0.04	0.30	0.04	0.33	0.04	0.33	0.04	0.31	0.03	0.35	0.04
1645	2	0.28	0.04	0.31	0.04	0.30	0.04	0.30	0.04	0.32	0.04	0.31	0.03	0.33	0.04	0.37	0.04
1670	2	0.28	0.04	0.30	0.04	0.31	0.04	0.28	0.04	0.31	0.04	0.31	0.04	0.33	0.04	0.32	0.04
1695	2	0.30	0.04	0.30	0.04	0.30	0.04	0.30	0.04	0.31	0.04	0.33	0.04	0.35	0.04	0.35	0.04
1720	2	0.28	0.04	0.29	0.04	0.29	0.04	0.25	0.03	0.29	0.03	0.34	0.04	0.33	0.04	0.34	0.04

1745	2	0.26	0.03	0.27	0.04	0.27	0.04	0.28	0.04	0.31	0.03	0.31	0.03	0.35	0.04	0.34	0.04
1770	2	0.31	0.04	0.31	0.04	0.28	0.04	0.28	0.04	0.34	0.04	0.34	0.04	0.33	0.04	0.37	0.04
1795	2	0.27	0.03	0.27	0.04	0.28	0.04	0.30	0.04	0.29	0.03	0.30	0.03	0.33	0.04	0.33	0.04
1820	2	0.28	0.04	0.30	0.04	0.26	0.03	0.32	0.04	0.29	0.03	0.27	0.03	0.31	0.04	0.35	0.04
1845	2	0.28	0.04	0.32	0.04	0.27	0.03	0.25	0.03	0.26	0.03	0.28	0.03	0.33	0.04	0.29	0.03
1870	2	0.27	0.03	0.26	0.03	0.27	0.03	0.28	0.04	0.29	0.03	0.29	0.03	0.31	0.04	0.31	0.04
1895	2	0.22	0.03	0.23	0.03	0.27	0.03	0.27	0.03	0.31	0.04	0.32	0.04	0.34	0.04	0.31	0.04
1920	2	0.28	0.04	0.24	0.03	0.30	0.04	0.25	0.03	0.28	0.03	0.28	0.03	0.32	0.04	0.31	0.05
1945	2	0.23	0.03	0.22	0.03	0.25	0.03	0.24	0.03	0.26	0.03	0.26	0.03	0.29	0.03	0.30	0.05
1970	2	0.25	0.03	0.28	0.04	0.27	0.04	0.23	0.03	0.26	0.03	0.29	0.03	0.29	0.03	0.30	0.05
1995	2	0.26	0.03	0.24	0.03	0.25	0.03	0.24	0.03	0.24	0.03	0.30	0.04	0.29	0.04	0.30	0.05

Table 2

E_{lab} (keV)	$\sigma_{E_{lab}}$ (keV)	($\sigma \pm d\sigma$) (mb/sr), P_2															
		135°		140°		145°		150°		155°		160°		165°		170°	
894	2	0.55	0.07	0.50	0.06	0.48	0.06	0.44	0.06	0.51	0.06	0.51	0.06	0.48	0.05	0.45	0.05
919	2	0.55	0.07	0.60	0.07	0.51	0.06	0.53	0.07	0.49	0.06	0.54	0.06	0.56	0.06	0.60	0.07
944	2	0.52	0.06	0.54	0.07	0.58	0.07	0.59	0.07	0.61	0.07	0.62	0.07	0.62	0.07	0.48	0.05
967	2	0.58	0.07	0.60	0.07	0.61	0.08	0.62	0.08	0.62	0.07	0.66	0.07	0.70	0.08	0.67	0.07
994	2	0.65	0.06	0.59	0.07	0.66	0.08	0.67	0.08	0.63	0.07	0.70	0.08	0.76	0.08	0.71	0.08
1019	2	0.65	0.08	0.68	0.08	0.69	0.08	0.70	0.09	0.70	0.07	0.68	0.07	0.80	0.08	0.75	0.08
1044	2	0.73	0.09	0.72	0.09	0.74	0.09	0.73	0.09	0.80	0.09	0.79	0.08	0.85	0.09	0.81	0.09
1069	2	0.73	0.09	0.78	0.10	0.72	0.09	0.74	0.09	0.76	0.08	0.82	0.09	0.89	0.09	0.86	0.09
1094	2	0.78	0.10	0.73	0.09	0.74	0.09	0.79	0.10	0.80	0.09	0.82	0.09	0.91	0.10	0.95	0.10
1119	2	0.78	0.09	0.71	0.09	0.76	0.09	0.78	0.09	0.87	0.09	0.81	0.09	0.91	0.10	0.97	0.10
1144	2	0.78	0.09	0.79	0.10	0.81	0.10	0.83	0.10	0.88	0.09	0.90	0.09	1.00	0.10	0.94	0.10
1169	2	0.86	0.10	0.87	0.11	0.86	0.10	0.86	0.10	0.91	0.10	0.95	0.10	1.03	0.11	1.02	0.11
1194	2	0.81	0.10	0.86	0.10	0.83	0.10	0.90	0.11	0.96	0.10	0.99	0.10	1.05	0.11	1.17	0.12
1219	2	0.84	0.10	0.92	0.11	0.92	0.12	0.91	0.11	0.96	0.10	1.03	0.11	1.17	0.12	1.06	0.11
1244	2	0.95	0.11	0.96	0.12	0.90	0.11	0.93	0.11	1.05	0.11	1.05	0.11	1.16	0.12	1.24	0.13

1269	2	0.84	0.10	0.83	0.10	0.92	0.11	0.98	0.12	1.06	0.11	1.07	0.11	1.20	0.13	1.16	0.12
1294	2	0.82	0.10	0.84	0.10	0.92	0.11	0.98	0.12	1.08	0.11	1.02	0.11	1.18	0.12	1.12	0.12
1319	2	0.86	0.10	0.91	0.11	0.91	0.11	0.97	0.12	1.14	0.12	1.01	0.11	1.24	0.13	1.20	0.13
1344	2	0.91	0.11	0.93	0.11	0.95	0.11	1.00	0.12	1.06	0.11	1.09	0.11	1.13	0.12	1.20	0.13
1369	2	0.92	0.11	0.87	0.11	0.99	0.12	1.02	0.12	1.10	0.12	1.06	0.11	1.18	0.13	1.24	0.13
1394	2	0.82	0.10	0.92	0.11	0.95	0.12	1.01	0.12	1.10	0.12	1.09	0.12	1.18	0.13	1.20	0.13
1419	2	0.90	0.11	0.95	0.12	0.94	0.11	1.01	0.12	1.07	0.11	1.11	0.12	1.12	0.12	1.23	0.13
1444	2	0.91	0.11	0.92	0.11	0.95	0.12	0.98	0.12	1.04	0.11	1.04	0.11	1.18	0.12	1.19	0.13
1469	2	0.92	0.11	0.95	0.12	0.99	0.12	0.99	0.12	1.19	0.13	1.09	0.11	1.13	0.12	1.26	0.13
1494	2	1.01	0.12	1.08	0.13	1.02	0.12	1.05	0.13	1.23	0.13	1.24	0.13	1.27	0.14	1.31	0.14
1520	2	1.04	0.13	1.06	0.13	1.08	0.13	1.08	0.13	1.19	0.13	1.23	0.13	1.30	0.14	1.30	0.14
1545	2	1.06	0.13	1.08	0.13	1.13	0.14	1.09	0.13	1.20	0.13	1.24	0.13	1.27	0.14	1.36	0.14
1570	2	1.04	0.13	1.05	0.13	1.12	0.14	1.21	0.15	1.23	0.13	1.35	0.14	1.37	0.15	1.54	0.16
1595	2	1.12	0.14	1.24	0.15	1.16	0.14	1.21	0.15	1.37	0.15	1.37	0.15	1.45	0.15	1.55	0.17
1620	2	1.12	0.14	1.21	0.15	1.18	0.14	1.27	0.15	1.32	0.14	1.40	0.15	1.43	0.15	1.56	0.17
1645	2	1.12	0.14	1.21	0.15	1.20	0.15	1.25	0.15	1.36	0.15	1.52	0.16	1.56	0.17	1.54	0.16
1670	2	1.18	0.15	1.31	0.16	1.24	0.15	1.37	0.17	1.42	0.15	1.50	0.16	1.55	0.17	1.61	0.17
1695	2	1.24	0.15	1.27	0.16	1.25	0.15	1.37	0.17	1.51	0.16	1.54	0.16	1.67	0.18	1.64	0.17
1720	2	1.34	0.16	1.30	0.16	1.36	0.17	1.36	0.17	1.54	0.16	1.66	0.18	1.70	0.18	1.68	0.18

1745	2	1.29	0.16	1.37	0.17	1.46	0.18	1.50	0.18	1.68	0.18	1.69	0.18	1.81	0.19	1.84	0.19
1770	2	1.42	0.17	1.45	0.18	1.49	0.18	1.45	0.18	1.73	0.18	1.68	0.18	1.84	0.20	1.85	0.20
1795	2	1.40	0.17	1.43	0.17	1.39	0.17	1.51	0.18	1.72	0.18	1.71	0.18	1.79	0.19	1.85	0.20
1820	2	1.35	0.17	1.40	0.17	1.43	0.18	1.51	0.19	1.68	0.18	1.76	0.19	1.90	0.20	1.96	0.21
1845	2	1.46	0.18	1.46	0.18	1.49	0.18	1.53	0.19	1.71	0.18	1.72	0.19	1.85	0.20	1.92	0.20
1870	2	1.45	0.18	1.51	0.19	1.54	0.19	1.65	0.20	1.76	0.19	1.79	0.19	1.87	0.20	1.97	0.21
1895	2	1.47	0.18	1.55	0.19	1.52	0.19	1.61	0.20	1.78	0.19	1.79	0.19	2.02	0.21	1.98	0.21
1920	2	1.38	0.17	1.53	0.19	1.53	0.19	1.63	0.20	1.68	0.17	1.90	0.20	1.95	0.21	1.98	0.21
1945	2	1.36	0.17	1.53	0.19	1.47	0.18	1.65	0.20	1.75	0.18	1.87	0.20	1.93	0.21	1.92	0.20
1970	2	1.49	0.18	1.56	0.19	1.55	0.19	1.66	0.20	1.84	0.20	1.79	0.19	2.02	0.21	2.06	0.22
1995	2	1.55	0.19	1.51	0.19	1.45	0.18	1.58	0.19	1.74	0.19	1.84	0.20	1.93	0.21	1.95	0.21

Table 3

E_{lab} (keV)	$\sigma_{E_{lab}}$ (keV)	$(\sigma \pm d\sigma)$ (mb/sr), p_3															
		135°		140°		145°		150°		155°		160°		165°		170°	
894	2	0.214	0.028	0.184	0.028	0.161	0.020	0.197	0.026	0.197	0.024	0.197	0.024	0.199	0.023	0.163	0.022
919	2	0.23	0.03	0.171	0.027	0.22	0.03	0.220	0.029	0.169	0.022	0.244	0.029	0.192	0.024	0.204	0.025
944	2	0.25	0.03	0.23	0.03	0.22	0.03	0.228	0.03	0.199	0.024	0.246	0.028	0.189	0.023	0.229	0.027
967	2	0.25	0.03	0.25	0.04	0.24	0.03	0.23	0.03	0.244	0.028	0.234	0.024	0.220	0.026	0.226	0.026
994	2	0.30	0.04	0.22	0.03	0.24	0.03	0.26	0.03	0.206	0.026	0.219	0.026	0.249	0.028	0.253	0.029
1019	2	0.29	0.03	0.26	0.03	0.27	0.03	0.24	0.03	0.25	0.03	0.27	0.03	0.259	0.028	0.228	0.028
1044	2	0.33	0.04	0.35	0.05	0.29	0.04	0.29	0.04	0.25	0.03	0.27	0.03	0.28	0.03	0.28	0.03
1069	2	0.33	0.04	0.26	0.03	0.27	0.04	0.28	0.04	0.28	0.03	0.31	0.04	0.28	0.03	0.27	0.03
1094	2	0.34	0.04	0.32	0.04	0.30	0.04	0.32	0.04	0.26	0.03	0.30	0.03	0.30	0.03	0.27	0.03
1119	2	0.34	0.04	0.37	0.05	0.35	0.04	0.35	0.04	0.28	0.03	0.28	0.03	0.28	0.03	0.30	0.03
1144	2	0.36	0.05	0.33	0.04	0.35	0.04	0.31	0.04	0.32	0.04	0.31	0.03	0.33	0.04	0.29	0.03
1169	2	0.38	0.05	0.38	0.05	0.35	0.04	0.32	0.04	0.32	0.04	0.31	0.03	0.31	0.03	0.33	0.04
1194	2	0.42	0.05	0.40	0.05	0.37	0.04	0.36	0.04	0.35	0.04	0.32	0.04	0.32	0.03	0.34	0.04
1219	2	0.39	0.05	0.37	0.05	0.37	0.05	0.34	0.04	0.34	0.04	0.34	0.04	0.33	0.04	0.34	0.04
1244	2	0.40	0.05	0.39	0.05	0.37	0.05	0.35	0.04	0.35	0.04	0.35	0.04	0.37	0.04	0.33	0.04

1269	2	0.41	0.05	0.42	0.05	0.41	0.05	0.38	0.05	0.32	0.04	0.36	0.04	0.35	0.04	0.32	0.04
1294	2	0.41	0.05	0.42	0.05	0.37	0.05	0.38	0.05	0.37	0.04	0.39	0.04	0.39	0.04	0.34	0.04
1319	2	0.42	0.05	0.47	0.06	0.38	0.05	0.39	0.05	0.36	0.04	0.40	0.04	0.35	0.04	0.40	0.04
1344	2	0.45	0.06	0.40	0.05	0.40	0.05	0.39	0.05	0.37	0.04	0.35	0.04	0.38	0.04	0.41	0.05
1369	2	0.52	0.06	0.43	0.06	0.44	0.06	0.41	0.05	0.43	0.05	0.39	0.04	0.41	0.04	0.40	0.05
1394	2	0.50	0.06	0.48	0.06	0.46	0.06	0.46	0.06	0.41	0.05	0.37	0.04	0.40	0.04	0.38	0.04
1419	2	0.49	0.06	0.47	0.06	0.47	0.06	0.44	0.05	0.47	0.05	0.43	0.05	0.43	0.05	0.42	0.05
1444	2	0.58	0.07	0.48	0.06	0.48	0.06	0.45	0.06	0.43	0.05	0.43	0.05	0.46	0.05	0.43	0.05
1469	2	0.54	0.07	0.54	0.07	0.49	0.06	0.48	0.06	0.53	0.06	0.43	0.05	0.47	0.05	0.45	0.05
1494	2	0.54	0.07	0.58	0.07	0.50	0.06	0.49	0.06	0.48	0.06	0.47	0.05	0.49	0.05	0.46	0.05
1520	2	0.60	0.07	0.56	0.07	0.54	0.07	0.51	0.06	0.50	0.06	0.49	0.06	0.55	0.06	0.47	0.05
1545	2	0.58	0.07	0.61	0.08	0.57	0.07	0.54	0.07	0.53	0.06	0.47	0.06	0.48	0.05	0.50	0.06
1570	2	0.65	0.08	0.54	0.07	0.54	0.07	0.55	0.07	0.46	0.05	0.47	0.05	0.48	0.05	0.48	0.05
1595	2	0.59	0.07	0.64	0.08	0.55	0.07	0.51	0.06	0.51	0.06	0.48	0.06	0.49	0.05	0.53	0.06
1620	2	0.63	0.08	0.54	0.07	0.56	0.07	0.49	0.06	0.45	0.05	0.49	0.06	0.43	0.05	0.51	0.06
1645	2	0.58	0.07	0.56	0.07	0.52	0.07	0.53	0.06	0.47	0.06	0.45	0.05	0.45	0.05	0.47	0.06
1670	2	0.61	0.08	0.54	0.07	0.49	0.06	0.50	0.06	0.50	0.06	0.43	0.05	0.45	0.05	0.45	0.05
1695	2	0.63	0.08	0.55	0.07	0.55	0.07	0.49	0.06	0.47	0.05	0.44	0.05	0.43	0.05	0.47	0.05
1720	2	0.61	0.08	0.59	0.07	0.52	0.07	0.44	0.05	0.46	0.05	0.42	0.05	0.40	0.04	0.48	0.06

1745	2	0.54	0.07	0.55	0.07	0.46	0.06	0.46	0.06	0.49	0.06	0.41	0.05	0.39	0.04	0.43	0.05
1770	2	0.60	0.08	0.50	0.07	0.50	0.07	0.50	0.06	0.43	0.05	0.35	0.05	0.43	0.05	0.37	0.05
1795	2	0.54	0.07	0.50	0.07	0.51	0.07	0.46	0.06	0.43	0.05	0.34	0.04	0.39	0.04	0.39	0.05
1820	2	0.53	0.07	0.51	0.07	0.51	0.07	0.45	0.06	0.38	0.05	0.33	0.05	0.41	0.04	0.32	0.05
1845	2	0.55	0.07	0.52	0.07	0.47	0.06	0.44	0.06	0.42	0.05	0.32	0.05	0.39	0.04	0.39	0.05
1870	2	0.58	0.08	0.49	0.07	0.44	0.06	0.44	0.06	0.35	0.05	0.36	0.06	0.39	0.04	0.35	0.05
1895	2	0.55	0.07	0.47	0.06	0.49	0.07	0.42	0.05	0.39	0.05	0.34	0.05	0.39	0.04	0.30	0.05
1920	2	0.50	0.07	0.51	0.07	0.43	0.06	0.43	0.05	0.36	0.05	0.36	0.05	0.36	0.04	0.34	0.05
1945	2	0.46	0.06	0.46	0.06	0.43	0.06	0.44	0.06	0.38	0.05	0.34	0.05	0.37	0.05	0.26	0.04
1970	2	0.53	0.07	0.52	0.07	0.45	0.06	0.40	0.06	0.36	0.05	0.36	0.05	0.40	0.05	0.32	0.05
1995	2	0.53	0.07	0.48	0.07	0.47	0.06	0.38	0.05	0.33	0.05	0.36	0.05	0.36	0.05	0.35	0.05

Table 4

E_{lab} (keV)	$\sigma_{E_{lab}}$ (keV)	$(\sigma \pm d\sigma)$ (mb/sr), p_{45}															
		135°		140°		145°		150°		155°		160°		165°		170°	
894	2	1.01	0.12	0.92	0.11	1.11	0.14	0.93	0.12	1.11	0.12	1.07	0.11	1.24	0.13	1.21	0.13
919	2	1.05	0.11	1.11	0.14	1.12	0.14	1.16	0.14	1.29	0.14	1.31	0.11	1.29	0.14	1.47	0.16
944	2	1.13	0.14	1.12	0.14	1.17	0.14	1.25	0.15	1.28	0.14	1.32	0.14	1.38	0.15	1.44	0.15
967	2	1.14	0.14	1.19	0.15	1.19	0.15	1.31	0.16	1.34	0.14	1.38	0.15	1.50	0.16	1.52	0.16
994	2	1.24	0.15	1.26	0.15	1.24	0.15	1.38	0.17	1.37	0.15	1.47	0.16	1.53	0.16	1.70	0.18
1019	2	1.23	0.15	1.40	0.17	1.37	0.17	1.37	0.17	1.56	0.16	1.62	0.17	1.65	0.17	1.80	0.19
1044	2	1.44	0.17	1.45	0.18	1.50	0.18	1.55	0.19	1.61	0.17	1.81	0.19	1.85	0.19	1.86	0.19
1069	2	1.47	0.18	1.52	0.18	1.51	0.18	1.55	0.19	1.66	0.17	1.82	0.19	1.90	0.20	2.03	0.21
1094	2	1.48	0.18	1.43	0.17	1.62	0.20	1.69	0.20	1.81	0.19	1.81	0.18	1.96	0.21	2.14	0.22
1119	2	1.54	0.18	1.56	0.19	1.62	0.19	1.78	0.21	1.89	0.20	1.80	0.18	2.09	0.22	2.06	0.21
1144	2	1.62	0.19	1.68	0.20	1.77	0.21	1.73	0.21	2.06	0.21	1.96	0.20	2.22	0.23	2.17	0.22
1169	2	1.73	0.21	1.73	0.21	1.83	0.22	1.87	0.22	2.03	0.21	2.06	0.21	2.22	0.23	2.29	0.24
1194	2	1.78	0.21	1.97	0.23	1.91	0.23	1.98	0.24	2.17	0.22	2.30	0.24	2.27	0.24	2.28	0.24
1219	2	1.77	0.21	1.97	0.24	1.87	0.22	2.07	0.25	2.34	0.24	2.34	0.24	2.41	0.25	2.51	0.26
1244	2	1.85	0.22	1.92	0.23	2.14	0.25	2.16	0.26	2.30	0.24	2.37	0.25	2.50	0.26	2.55	0.26

1269	2	1.95	0.23	2.12	0.25	2.17	0.26	2.08	0.25	2.22	0.23	2.42	0.25	2.54	0.27	2.61	0.27
1294	2	1.93	0.23	2.10	0.25	2.07	0.25	2.20	0.26	2.38	0.25	2.51	0.26	2.58	0.27	2.57	0.27
1319	2	2.05	0.24	2.19	0.26	2.25	0.27	2.35	0.28	2.53	0.26	2.58	0.27	2.84	0.29	2.66	0.28
1344	2	2.22	0.27	2.38	0.28	2.29	0.27	2.32	0.28	2.57	0.27	2.56	0.27	2.82	0.29	2.9	0.3
1369	2	2.24	0.27	2.25	0.27	2.36	0.28	2.6	0.3	2.75	0.29	2.68	0.28	2.9	0.3	3.0	0.3
1394	2	2.33	0.28	2.42	0.29	2.5	0.3	2.6	0.3	2.70	0.28	2.70	0.28	3.0	0.3	3.0	0.3
1419	2	2.39	0.29	2.5	0.3	2.6	0.3	2.6	0.3	2.78	0.29	2.81	0.29	3.0	0.3	3.1	0.3
1444	2	2.45	0.29	2.5	0.3	2.5	0.3	2.7	0.3	2.9	0.3	2.9	0.3	3.1	0.3	3.1	0.3
1469	2	2.6	0.3	2.6	0.3	2.8	0.3	2.8	0.3	3.0	0.3	3.0	0.3	3.2	0.3	3.2	0.3
1494	2	2.7	0.3	2.7	0.3	2.8	0.3	2.9	0.4	3.2	0.3	3.1	0.3	3.4	0.4	3.3	0.3
1520	2	2.8	0.3	2.9	0.3	2.9	0.4	3.0	0.4	3.1	0.3	3.2	0.3	3.3	0.3	3.3	0.3
1545	2	2.9	0.4	2.9	0.4	3.1	0.4	3.0	0.4	3.2	0.3	3.3	0.3	3.5	0.4	3.5	0.4
1570	2	2.9	0.4	3.2	0.4	3.1	0.4	3.2	0.4	3.4	0.4	3.4	0.4	3.7	0.4	3.6	0.4
1595	2	3.0	0.4	3.1	0.4	3.1	0.4	3.2	0.4	3.3	0.3	3.4	0.4	3.6	0.4	3.7	0.4
1620	2	2.9	0.4	3.1	0.4	3.1	0.4	3.1	0.4	3.3	0.3	3.4	0.4	3.6	0.4	3.7	0.4
1645	2	3.0	0.4	3.0	0.4	3.1	0.4	3.2	0.4	3.4	0.4	3.4	0.4	3.6	0.4	3.7	0.4
1670	2	3.0	0.4	3.1	0.4	3.1	0.4	3.2	0.4	3.3	0.4	3.5	0.4	3.7	0.4	3.7	0.4
1695	2	3.0	0.4	3.2	0.4	3.1	0.4	3.3	0.4	3.4	0.4	3.3	0.3	3.6	0.4	3.7	0.4
1720	2	3.2	0.4	3.2	0.4	3.3	0.4	3.2	0.4	3.5	0.4	3.5	0.4	3.8	0.4	3.9	0.4

1745	2	3.2	0.4	3.2	0.4	3.2	0.4	3.4	0.4	3.4	0.4	3.5	0.4	3.8	0.4	3.7	0.4
1770	2	3.2	0.4	3.3	0.4	3.4	0.4	3.4	0.4	3.6	0.4	3.6	0.4	4.0	0.4	3.8	0.4
1795	2	3.3	0.4	3.4	0.4	3.4	0.4	3.3	0.4	3.5	0.4	3.6	0.4	3.9	0.4	4.0	0.4
1820	2	3.2	0.4	3.3	0.4	3.4	0.4	3.5	0.4	3.7	0.4	3.8	0.4	4.1	0.4	4.0	0.4
1845	2	3.4	0.4	3.6	0.4	3.4	0.4	3.5	0.4	3.8	0.4	3.8	0.4	3.9	0.4	4.1	0.4
1870	2	3.5	0.4	3.6	0.4	3.5	0.4	3.6	0.4	3.9	0.4	3.8	0.4	4.2	0.4	4.0	0.4
1895	2	3.6	0.4	3.6	0.4	3.6	0.4	3.7	0.4	4.0	0.4	4.0	0.4	4.2	0.4	4.3	0.5
1920	2	3.6	0.4	3.7	0.4	3.6	0.4	3.8	0.5	3.9	0.4	3.9	0.4	4.2	0.4	4.2	0.4
1945	2	3.4	0.4	3.7	0.4	3.4	0.4	3.7	0.4	3.8	0.4	4.0	0.4	4.0	0.4	4.4	0.5
1970	2	3.7	0.4	3.7	0.5	3.7	0.4	3.9	0.5	4.0	0.4	4.1	0.4	4.4	0.5	4.4	0.5
1995	2	3.6	0.4	3.8	0.5	3.5	0.4	3.8	0.5	4.1	0.4	3.9	0.4	4.2	0.4	4.1	0.4

Table 5

E_{lab} (keV)	$\sigma_{E_{lab}}$ (keV)	($\sigma \pm d\sigma$) (mb/sr), p_6															
		135°		140°		145°		150°		155°		160°		165°		170°	
1094	2	0.72	0.09	0.71	0.09	0.77	0.10	0.73	0.09	0.82	0.09	0.83	0.09	0.94	0.10	0.95	0.10
1119	2	0.75	0.09	0.69	0.08	0.67	0.08	0.70	0.09	0.87	0.09	0.87	0.09	0.97	0.10	0.96	0.10
1144	2	0.83	0.10	0.82	0.10	0.75	0.09	0.76	0.09	0.96	0.10	0.94	0.10	1.00	0.11	1.00	0.11
1169	2	0.83	0.10	0.91	0.11	0.81	0.10	0.80	0.10	0.95	0.10	0.95	0.10	1.00	0.11	1.05	0.11
1194	2	0.90	0.11	0.93	0.11	0.85	0.10	0.88	0.11	1.04	0.11	1.09	0.11	1.03	0.11	1.16	0.12
1219	2	0.92	0.11	0.94	0.11	0.91	0.11	0.94	0.12	1.01	0.11	1.12	0.12	1.14	0.12	1.17	0.12
1244	2	0.96	0.12	0.96	0.12	0.97	0.12	0.95	0.12	1.10	0.12	1.11	0.12	1.20	0.13	1.25	0.13
1269	2	0.92	0.11	0.99	0.12	0.99	0.12	0.96	0.12	1.08	0.11	1.15	0.12	1.24	0.13	1.25	0.13
1294	2	0.96	0.12	0.97	0.12	0.95	0.11	1.04	0.13	1.08	0.11	1.09	0.11	1.22	0.13	1.27	0.13
1319	2	0.99	0.12	1.02	0.12	1.03	0.13	1.09	0.13	1.22	0.13	1.16	0.12	1.33	0.14	1.30	0.14
1344	2	0.98	0.12	1.06	0.13	1.00	0.12	1.15	0.14	1.22	0.13	1.24	0.13	1.27	0.13	1.36	0.14
1369	2	1.04	0.13	1.07	0.13	1.04	0.13	1.15	0.14	1.22	0.13	1.29	0.14	1.37	0.15	1.36	0.14
1394	2	1.07	0.13	1.15	0.14	1.09	0.13	1.22	0.15	1.25	0.13	1.33	0.14	1.44	0.15	1.43	0.15
1419	2	1.16	0.14	1.14	0.14	1.15	0.14	1.24	0.15	1.30	0.14	1.36	0.14	1.41	0.15	1.50	0.16
1444	2	1.19	0.14	1.22	0.15	1.16	0.14	1.30	0.16	1.35	0.14	1.33	0.14	1.45	0.15	1.58	0.16

1469	2	1.24	0.15	1.29	0.16	1.32	0.16	1.29	0.16	1.46	0.16	1.49	0.16	1.58	0.17	1.57	0.17
1494	2	1.29	0.16	1.36	0.17	1.33	0.16	1.37	0.17	1.54	0.16	1.49	0.16	1.59	0.17	1.68	0.18
1520	2	1.31	0.16	1.41	0.17	1.42	0.17	1.40	0.17	1.55	0.16	1.61	0.17	1.61	0.17	1.74	0.18
1545	2	1.41	0.17	1.36	0.16	1.41	0.17	1.43	0.18	1.52	0.16	1.52	0.16	1.65	0.17	1.73	0.18
1570	2	1.44	0.17	1.39	0.17	1.35	0.17	1.46	0.18	1.59	0.17	1.54	0.16	1.69	0.18	1.78	0.19
1595	2	1.38	0.17	1.34	0.16	1.43	0.17	1.55	0.19	1.62	0.17	1.49	0.16	1.67	0.18	1.75	0.18
1620	2	1.30	0.16	1.33	0.16	1.38	0.17	1.35	0.17	1.41	0.15	1.49	0.16	1.61	0.17	1.66	0.17
1645	2	1.33	0.16	1.36	0.17	1.33	0.16	1.41	0.17	1.46	0.15	1.46	0.15	1.63	0.17	1.61	0.17
1670	2	1.21	0.15	1.33	0.16	1.22	0.15	1.24	0.15	1.33	0.14	1.43	0.15	1.53	0.16	1.53	0.16
1695	2	1.21	0.15	1.28	0.16	1.21	0.15	1.26	0.15	1.31	0.14	1.40	0.15	1.38	0.15	1.51	0.16
1720	2	1.17	0.14	1.26	0.15	1.19	0.15	1.29	0.16	1.34	0.14	1.39	0.15	1.42	0.15	1.37	0.15
1745	2	1.22	0.15	1.15	0.14	1.15	0.14	1.18	0.15	1.24	0.13	1.24	0.13	1.39	0.15	1.41	0.15
1770	2	1.12	0.14	1.09	0.13	1.11	0.14	1.16	0.14	1.21	0.13	1.23	0.13	1.33	0.14	1.35	0.15
1795	2	1.06	0.13	1.11	0.14	1.04	0.13	0.98	0.12	1.21	0.13	1.15	0.12	1.25	0.13	1.27	0.14
1820	2	1.05	0.13	1.03	0.13	0.95	0.12	1.02	0.13	1.05	0.12	1.09	0.12	1.14	0.13	1.22	0.13
1845	2	1.02	0.13	1.03	0.13	0.94	0.12	0.90	0.11	1.08	0.12	1.05	0.12	1.07	0.12	1.10	0.12
1870	2	1.00	0.12	0.99	0.12	0.90	0.11	0.90	0.11	1.01	0.11	1.01	0.11	1.09	0.12	1.02	0.11
1895	2	-	-	0.87	0.11	0.93	0.12	0.94	0.12	0.97	0.11	0.98	0.11	1.05	0.12	0.98	0.11
1920	2	0.92	0.11	0.81	0.10	0.86	0.11	0.84	0.11	0.84	0.10	0.89	0.10	0.95	0.11	0.97	0.11

1945	2	0.80	0.10	0.84	0.11	0.73	0.09	0.75	0.10	0.76	0.08	0.79	0.09	0.82	0.09	0.89	0.10
1970	2	0.85	0.11	0.79	0.10	0.78	0.10	0.76	0.10	0.76	0.08	0.80	0.09	0.87	0.10	0.81	0.09
1995	2	0.78	0.10	0.73	0.09	0.69	0.4	0.62	0.08	0.71	0.08	0.72	0.08	0.70	0.08	0.75	0.08

Table 6

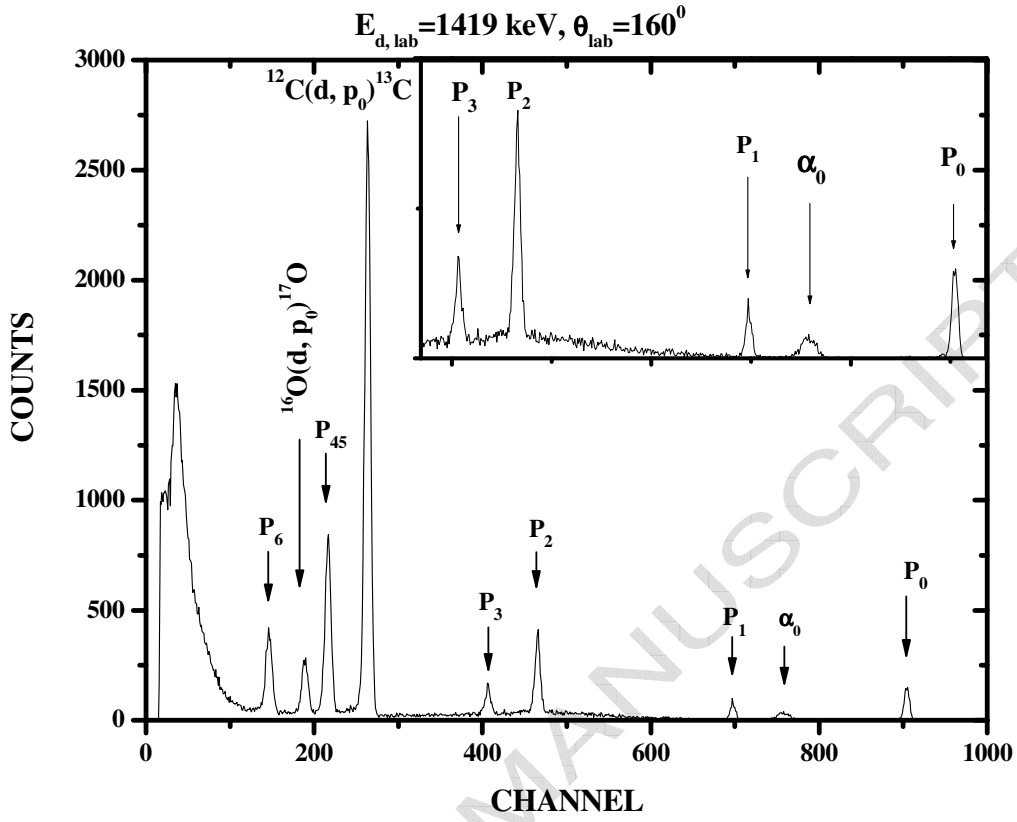

Fig. 1

Fig. 2a

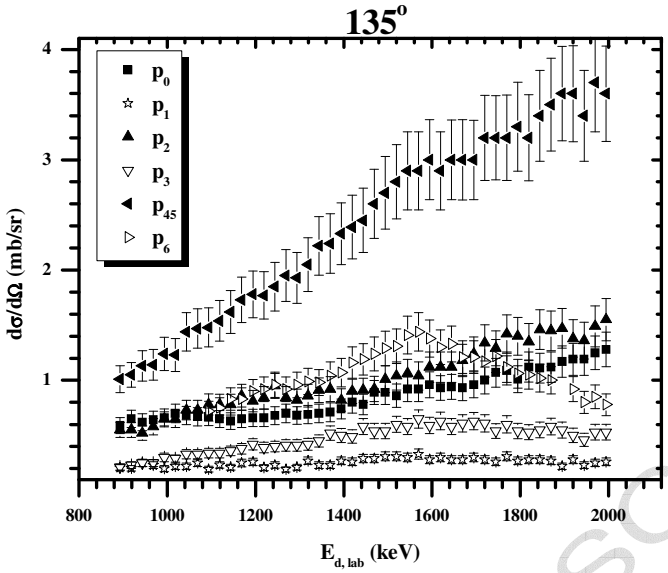

Fig. 2b

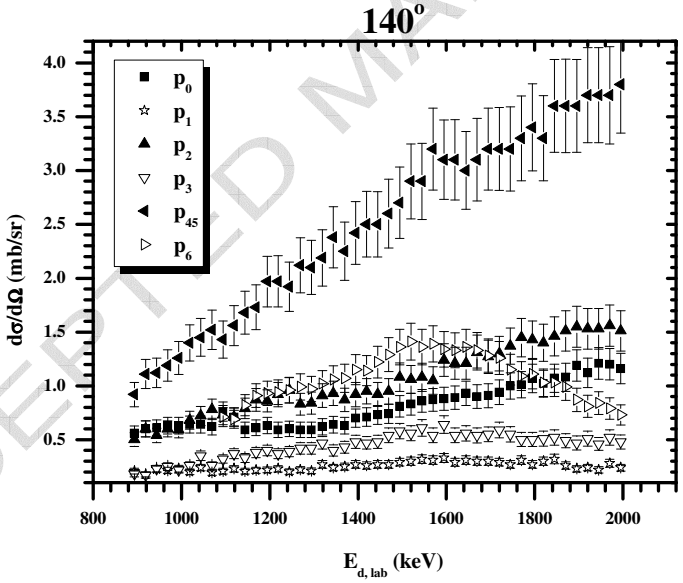

Fig. 2c

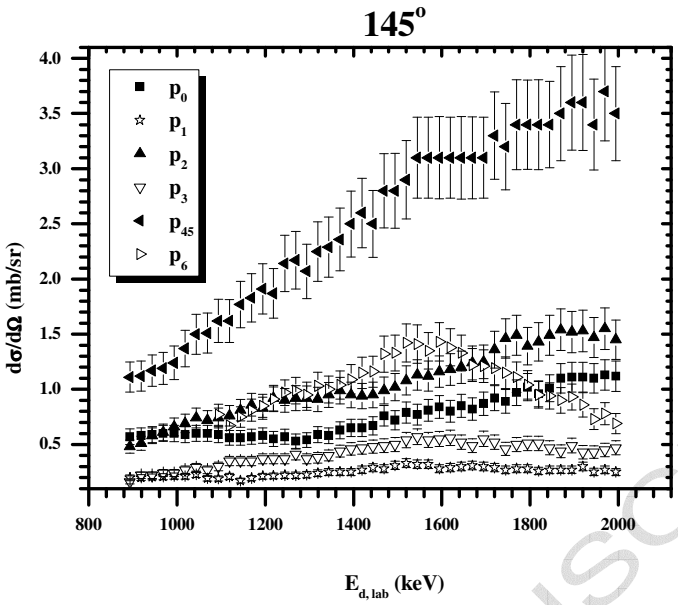

Fig. 2d

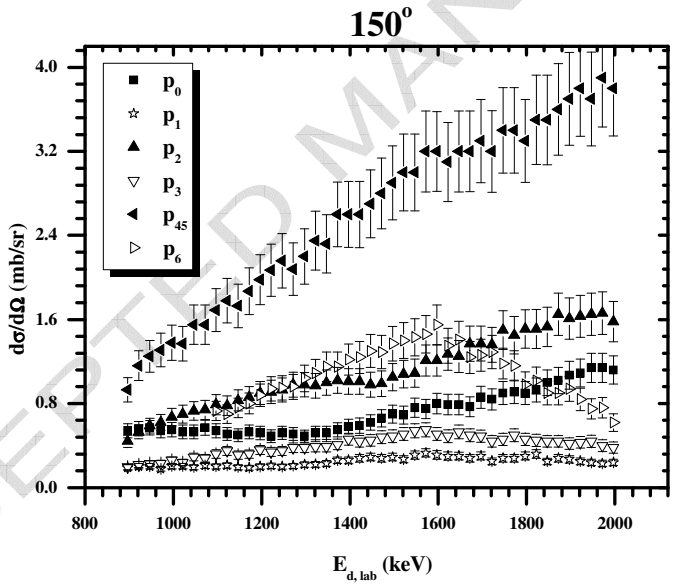

Fig. 2e

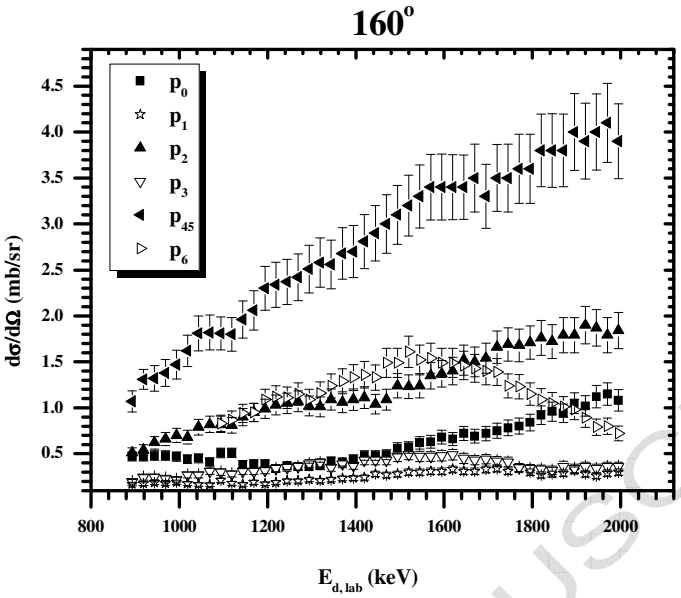

Fig. 2f

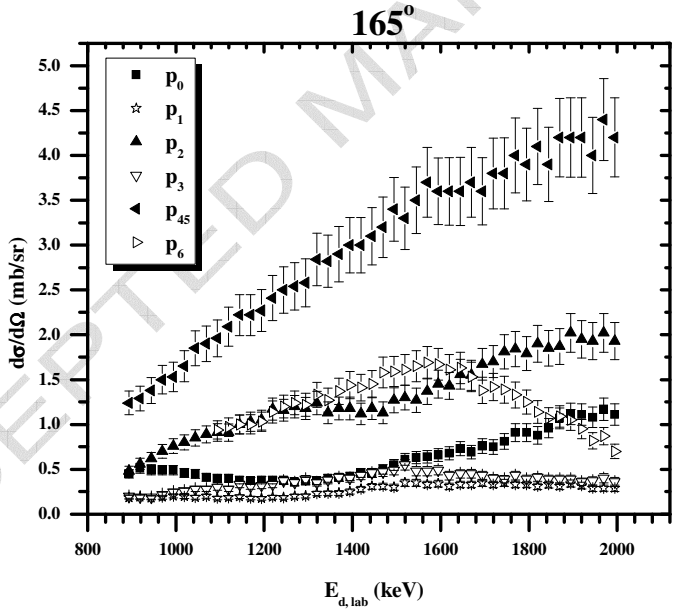

Fig. 2g

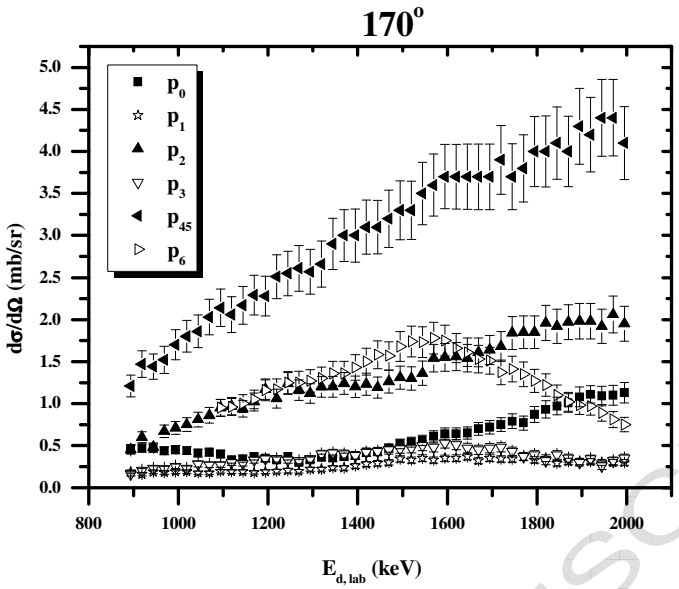

Fig. 3a

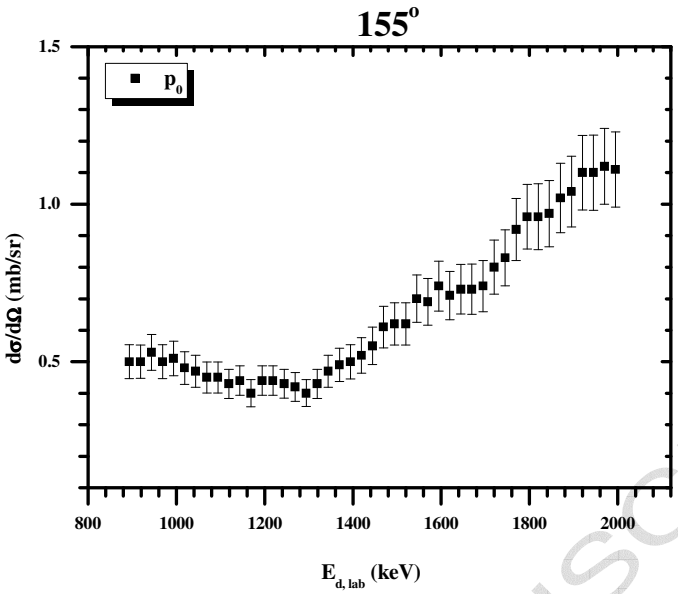

Fig. 3b

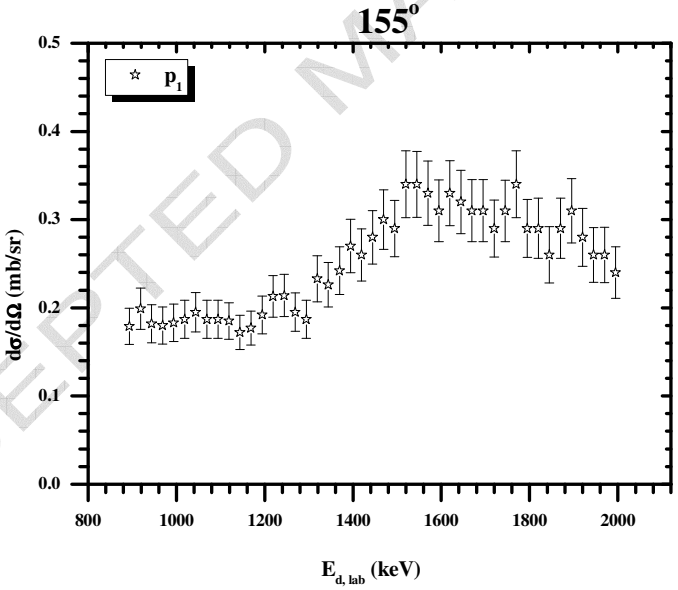

Fig. 3c

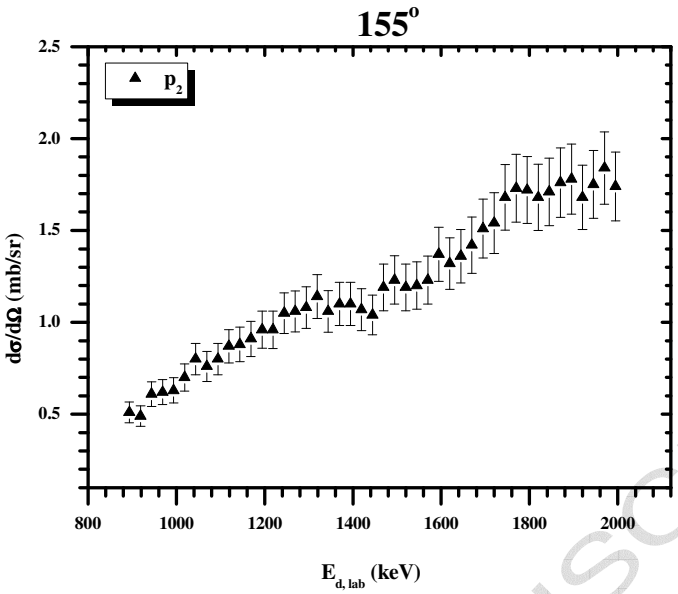

Fig. 3d

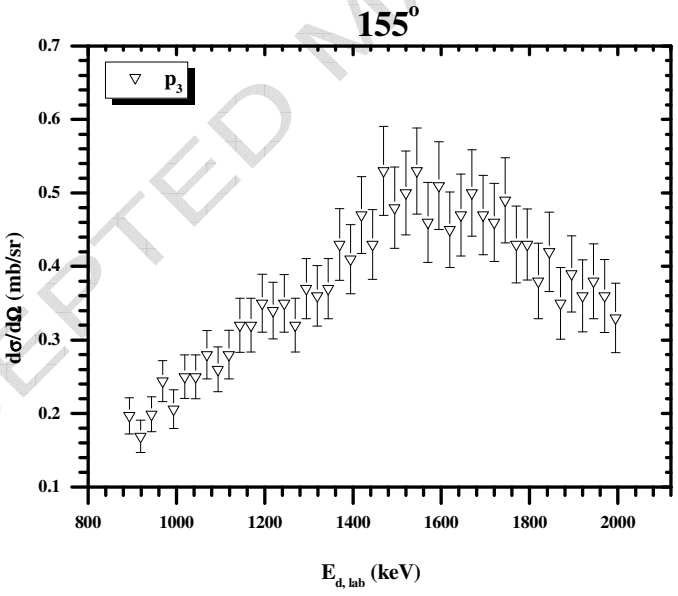

Fig. 3e

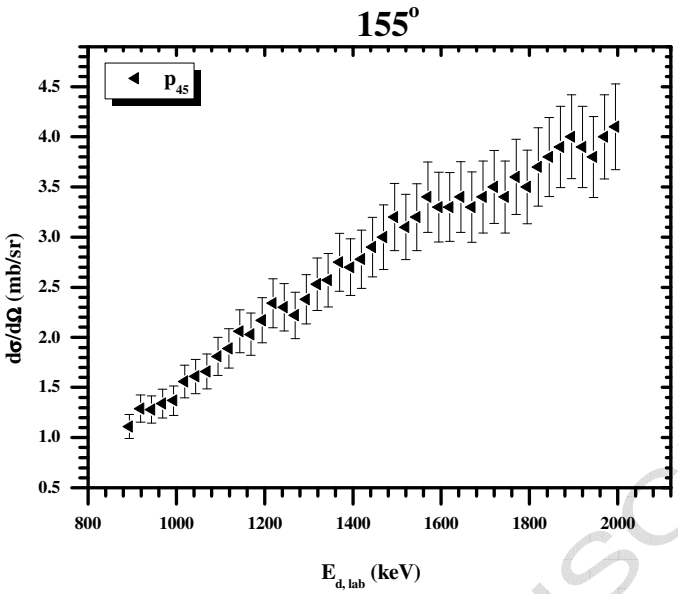

Fig. 3f